



Nb-doped TiO₂/carbon composite supports synthesized by ultrasonic spray pyrolysis for proton exchange membrane (PEM) fuel cell catalysts

Keerthi Senevirathne^{a,*,1}, Vladimir Neburchilov^a, Vanesa Alzate^a, Ryan Baker^a, Roberto Neagu^a, JiuJun Zhang^{a,*}, Stephen Campbell^b, Siyu Ye^c

^a National Research Council Canada, Institute for Fuel Cell Innovation, 4250 Westbrook Mall, Vancouver, BC V6T 1W5, Canada

^b AFCC Automotive Fuel Cell Cooperation Corp., Burnaby, BC V5J 5J8, Canada

^c Ballard Power Systems, Burnaby, BC V5J 5J8, Canada

H I G H L I G H T S

- ▶ Ultrasonic spray pyrolysis technique was employed to fabricate Nb doped TiO₂/carbon composites.
- ▶ Microwave assisted polyol reduction was used to deposit PtPd catalysts on USP synthesized supports.
- ▶ Nb-doped TiO₂/carbon composite materials are stable in acidic environment.
- ▶ Catalysts prepared using composite supports are 35% more active than commercial Pt/C catalysts.

A R T I C L E I N F O

Article history:

Received 2 June 2012

Received in revised form

20 July 2012

Accepted 23 July 2012

Available online 3 August 2012

Keywords:

Ultrasonic spray pyrolysis

Microwave-assisted polyol reduction

Nb-doped TiO₂

PtPd alloy catalysts

Oxygen reduction reaction

PEM fuel cells

A B S T R A C T

In this paper we report the use of both ultrasonic spray pyrolysis and microwave-assisted polyol reduction methods to synthesize Nb-doped TiO₂/carbon (25 wt% Nb_{0.07}Ti_{0.93}O₂/75 wt% carbon) composite supports and Pt_{0.62}Pd_{0.38} alloy catalysts, respectively. The physicochemical properties of the synthesized supports and their Pt_{0.62}Pd_{0.38} supported catalysts are evaluated using several methods including XRD, TEM, BET surface area analysis, TGA, as well as ICP-MS elemental analysis. The electronic conductivities and thermal/chemical stabilities of the supports are also evaluated with respect to their possible use as catalyst supports. Electrochemical measurements for oxygen reduction activity of the Pt_{0.62}Pd_{0.38} alloy catalysts supported on oxide/carbon composites are also carried out in order to check their suitability for possible PEM fuel cell applications. The results show that 20wt%Pt_{0.62}Pd_{0.38}/25 wt%(Nb_{0.07}Ti_{0.93}O₂)-75 wt%C catalysts exhibit enhanced mass activities compared to those of commercially available 48wt% Pt/C and home-made 20wt% Pt₆₂Pd₃₈/C catalysts.

© 2012 Elsevier B.V. All rights reserved.

1. Introduction

Proton exchange membrane (PEM) fuel cells have been recognized as a feasible energy technology for portable, stationary and transportation applications mainly due to their high energy-conversion efficiency, high power density, and low or zero emissions [1]. However, the main technical barriers such as insufficient catalyst durability and high cost, which are hindering the commercialization of PEM fuel cell technology, have been identified. The major factor causing these challenges is the low stability of catalysts.

At the current state of technology, the most practical PEM fuel cell catalysts are carbon supported Pt-based catalysts. There are two aspects, which can cause catalyst degradation. The first is Pt degradation induced by Pt dissolution and particle sintering, and the second is carbon support corrosion [2,3].

Carbon has been recognized as the most common catalyst support at the current state of technology state, due to its inherent high porosity, high surface area, and excellent electrical conductivity. However, severe carbon corrosion can take place in the presence of O₂ and at high cathode potential in acidic environment [4], in particular during the dynamic operation of the fuel cell. This carbon support corrosion will eventually lead to platinum (Pt) particle agglomeration and sintering, resulting in poor performance of the Pt catalyst. Moreover, carbon corrosion can also lead to electrically isolated catalyst particles that provide no contribution to catalyst activity. The end result is the short lifetime and poor performance of

* Corresponding authors. Tel.: +1 604 226 3000; fax: +1 604 221 3001.

E-mail addresses: senevirathne.k@gmail.com (K. Senevirathne), jiujun.zhang@nrc-nrc.gc.ca (J. Zhang).

¹ Wake Forest University, Department of Chemistry, Salem Hall, Gullet Drive, Winston-Salem, NC 27106, USA.

PEM fuel cell. In order to address these issues, efforts have been taken to develop alternative non-carbon supports. Some metal oxides have received much attention as alternative PEM fuel cell support materials due to their high chemical, thermal and electrochemical stability. Among the oxides, Nb- or Ta-doped TiO_2 has been a focus of study. In general, TiO_2 itself is not conductive enough to be employed as a catalyst support, therefore, high temperature reduction treatment in H_2 to create oxygen vacancies or introduction of dopants with higher oxidation state such as Nb^{5+} or Ta^{5+} are widely employed in order to yield a fraction of Ti^{3+} that help to enhance the electronic conductivity. Chevallier et al. [5] reported the synthesis of 5 at% Nb doped TiO_2 spheres by a polymer assisted method and its use as a PEM fuel cell catalyst support [5]. Bauer et al. [6] studied Nb doped TiO_2 nanofibers interlinked with carbon agglomerates as PEM fuel cell supports and reported a 0.34 W cm^{-2} peak power density at 75°C for single cell configuration [6]. Acid catalyzed sol–gel method has been successfully employed to synthesize Nb doped TiO_2 with high rutile content and conductivity, in which a correlation of increase in ORR activity with the increasing in conductivity was reported [7]. Unfortunately, although the ORR mass activity catalyzed by these metal oxides-supported catalysts had some extent of enhancement, their durability seemed to be not as good as those pure-carbon-supported catalysts. Therefore, continuing effort should be put on the improvement of the catalyst durability besides the further enhancement of their ORR mass activity.

Besides the catalyst stability improvement through developing alternative catalyst supports, the modifications to metal catalyst by alloying Pt with other metals has also been an approach in improving catalyst activity towards oxygen reduction reaction (ORR) because ORR is the dominant factor that accounts for fuel cell efficiency loss compared to anodic hydrogen oxidation reaction (HOR) [8]. Among Pt alloy catalysts, Pt–Pd alloys have shown some encouraging electrocatalytic properties [9,10].

In the effort to develop non-carbon supports and Pt alloy catalysts, catalyst synthesis plays a major role. Among the synthesis technologies for nano-scale materials, ultrasonic spray pyrolysis (USP), an aerosol processing technique, has been demonstrated to be a useful technique in catalyst support synthesis [11]. In this technique, a template, which has variety of sizes, is used, and subsequent removal of this template without disintegrating the structure can produce a material with high surface area and porosity, both of which can be adjusted by choosing the desired template. In this technique, a precursor solution mixed with an appropriate template is nebulized ultrasonically and the resultant mist is carried by a carrier gas through a glass or quartz tube placed in a heated furnace. The particle containing mist is allowed to condense and later collected by water-filled collecting vessel. Various porous materials such as metal oxides, carbon blacks, and silica/titania composite have been prepared by USP method using silica colloids as the template [12].

In this paper, we explored the USP method to synthesize metal oxide/carbon composite supports for ORR cathode catalysts in the effort to improve both the catalyst's ORR mass activity and durability. An alloy catalyst, Pt–Pd (3:1 ratio in weight or 0.62:0.38 in atomic ratio) was synthesized and supported on the metal oxide/carbon composite supports to form ORR catalysts. It is also worthwhile to indicate that to the best of our knowledge, this work should be the first attempt in synthesizing Nb-doped TiO_2 /carbon composite materials using USP technique.

2. Experimental

2.1. Support synthesis

In synthesizing metal/carbon composite support ($\text{Nb}_{0.07}\text{Ti}_{0.93}\text{O}_2$ /carbon (TKK-E), oxide/carbon ratio was 1:3 by weight) using

ultrasonic spray pyrolysis (USP) technique, TTK-E carbon was first treated in 5 M HNO_3 for 3 h at 100°C to introduce some surface functional groups and to increase hydrophilicity, followed by a vigorous washing with de-ionized water. A known amount of this pre-treated TTK-E (1.0 g) was then dispersed in 500 mL of de-ionized water by sonication for ~ 1.0 h with a probe sonicator (Misonix 3000) to form a carbon suspension. In a separate beaker, the required amount (for example, 1.8 mL) of Ti precursor, titanium(IV) bis-(ammonium lactate)dihydroxide ($\text{C}_6\text{H}_{18}\text{N}_2\text{O}_8\text{Ti}$, 50-wt % solution in water, purchased from Aldrich), and 85.4 mg of Nb precursor, ammonium niobate oxalate hydrate ($\text{C}_4\text{H}_4\text{NNbO}_9 \cdot x\text{H}_2\text{O}$, 99.99%, purchased from Aldrich) were dissolved in 20 mL of de-ionized water for 30 min by mechanical stirring to form a precursor solution. Then the carbon suspension with $\text{pH} \sim 2$ adjusted by using 1 M H_2SO_4 was added into this precursor solution and stirred for 2 h to form a homogeneous spray solution for USP synthesis.

The USP instrument used in this study consisted of three main components such as ultrasonic atomizer for aerosol generation, high temperature tube furnace (Carbolite (1200°C) with three zones temperature control) with a quartz tube, and water filled bubbler unit for sample collection. The ultrasonic spray unit mainly consists of the stainless steel sample chamber, which is fitted with four ultrasonic transducer modules (Sonaer Inc, New York) operating at a frequency of 2.4 MHz, refill tubing, and liquid level observation tube. This unit is connected by stainless steel fittings to the inlet of 1.7 m long quartz tube, which runs through the tube furnace. The outlet of this quartz tube was fitted to glass cylinder sample collectors each filled with ~ 150 mL of de-ionized water. The whole set up was flushed with argon for 2 h prior to introducing precursor solution.

For synthesizing $\text{Nb}_{0.07}\text{Ti}_{0.93}\text{O}_2$ /carbon composite support, the spray solution was placed in the ultrasonic spray chamber and purged with argon (flow rate $5 \text{ cm}^3 \text{ min}^{-1}$) for another 10 min to flush out remaining air in the precursor mixture prior to starting the transducers. Then, the transducers were turned on and the reaction was carried out under argon atmosphere at the desired synthesis temperature. The synthesized materials were then collected as an aqueous colloidal solution and isolated by centrifugation at 10,000 rpm for 15 min, and dried in a vacuum oven at 80°C until dry. As a post treatment, supports were reduced at 850°C in H_2 for 3 h. Note that the USP method mainly utilizes high frequency ultrasound to generate aerosol of a material of interest from a precursor solution. The size distribution, morphology of particles are some of the factors that depend on the concentration of precursor solution, velocity of aerosol droplets, frequency of atomizers etc [13]. In the literature, the USP method has been described as a convenient method of synthesizing spherical particles [12,14]. Nebulized precursor droplets travel through hot furnace several processes such as solidification and calcination, pyrolysis of organic components can take place.

In this paper, the synthesized support material is expressed as the formula of 25wt% ($\text{Nb}_{0.07}\text{Ti}_{0.93}\text{O}_2$) – 75wt% C, meaning that the support material contains 25 wt% of $\text{Nb}_{0.07}\text{Ti}_{0.93}\text{O}_2$, and 75 wt% of carbon (TKK-E).

2.2. Supported catalyst synthesis

PtPd alloy deposition on metal oxide/TKK-E hybrid supports was performed using microwave-assisted polyol reduction method. Briefly, a known amount of metal oxide/carbon support was first dispersed in anhydrous ethylene glycol by sonicating for 1 h in a sonicator bath followed by adjustment of $\text{pH} \sim 9$ –10 using 0.3 M NaOH in ethylene glycol. Next, the required amounts of chloroplatinic acid hexahydrate (H_2PtCl_6 , Sigma–Aldrich) and bis

ammonium chloropalladate ($(\text{NH}_4)_2\text{PdCl}_6$, Alfa Aesar) (with a target of 20-weight percent (20 wt%) Pt loading) were dissolved in minimum amount of ethylene glycol and de-ionized water, respectively, by sonication. The mixture of Pt and Pd precursor solutions was magnetically stirred for 15 min before addition into metal oxide/carbon dispersion. This mixture was stirred at room temperature for 1 h followed by microwave-assisted reduction. The heating process was carried out such that the solution was brought to boiling then heated at medium power with 10 s on and off cycles for 3 min. The prepared Pt-Pd catalyst was collected, and purified by filtration through Millipore filtration system (nitrocellulose membrane filter, 0.45 μm) and then washed with de-ionized water three times. Finally, the final catalyst powder sample was dried in an oven at 60 °C. In this paper, the synthesized catalyst is expressed as the formula of 20wt%Pt_{0.62}Pd_{0.38}/25wt% (Nb_{0.07}Ti_{0.93}O₂)-75 wt% C, meaning that the catalyst contains 20wt% of Pt_{0.62}Pd_{0.38}, and 80 wt% of (25 wt% (Nb_{0.07}Ti_{0.93}O₂)-75 wt% C) support.

2.3. Physical characterization of the supports and catalysts

2.3.1. XRD characterization

A Bruker AXS D8 Advance X-ray diffractometer (XRD) equipped with a Cu K α anode source (1.541838 Å) was used for X-ray powder diffraction analysis. A thin smear of vacuum grease was applied on zero background quartz (0001) holder followed by placing a uniform flat layer of powdered sample on top of the grease layer. The X-ray patterns were identified by matching with available phases in the EVA diffraction database.

2.3.2. TEM characterization

A Hitachi H7600 microscope, operated at 100 kV, was employed for imaging the USP synthesized samples. In the preparation of specimens, appropriate amount of powder was dispersed in ethanol by sonication in a sonicator bath for approximately 5 min followed by placing a drop of the resultant solution on a carbon-coated copper grid. The specimen was dried at room temperature prior to imaging under bright field mode.

2.3.3. TGA characterization for thermal stability

A Setaram TGA/DSC thermogravimetric analyzer was used to determine experimental carbon content in carbon/metal oxide hybrid supports. The heating profile was set such that the hybrid supports were heated up to 550 °C with a temperature ramp rate of 10 °C min⁻¹ and isothermally held at this temperature for 30 min followed by ramping up to 700 °C, in a continuous flow of air. The Setsys 2000 software was used to collect data. The weight loss was directly correlated to the weight of carbon in USP synthesized hybrid supports.

2.3.4. Surface area and porosity analysis

A Beckman Coulter SA 3100 Surface Area Analyzer was used in surface area and porosity analysis. Powder sample was out-gassed at 120 °C for 30 min prior to analysis. The specific surface area and pore size distribution of samples were evaluated using the Brunauer, Emmet, and Teller (BET) and the Barrett, Joyner, and Halenda (BJH) methods, respectively.

2.3.5. Conductivity measurement

Room temperature electronic conductivity measurements of 25 wt% (Nb_{0.07}Ti_{0.93}O₂)-75 wt% C powders were conducted using a specially designed gold-coated copper cell connected to a Solartron Analytical 1252A frequency response analyzer coupled with Solartron SI 1287 potentiostat electrochemical interface. A constant pressure (2.55 kg cm⁻²) was applied on the sample during the measurements in order to achieve proper contacts among the

support particles tested as well as between the gold-coated copper and the sample. The Z-plot and Z-view software were used to collect the bulk resistance data. The resistance of porous powders were measured and then converted into the conductivity. The conductivities obtained here should not reflect the materials' crystal conductivity values because the sample disks had a porous structure. This porous structure may be closer to that of an operating fuel cell's catalyst layers. Therefore, the conductivities reported here are those at specific conditions such as a stated fixed pressure and temperature.

2.3.6. Chemical stability measurement

For the evaluation of chemical stability of the synthesized support samples, the samples were tested according to the protocol outlined as follows: The niobium doped metal oxide support prepared without TTK-E carbon (0.2 g) was mixed with 50 mL of 1 M H₂SO₄ in a round bottom flask fitted with refluxing set up, and refluxed while stirring magnetically at 95 °C for 24 h in a silicone oil bath heated with a digitally controlled hot plate. After 24 h of refluxing, the solution and un-dissolved solid in the mixture were separated. Then, the collected solution was analyzed by elemental analysis (ICP/MS), and un-dissolved solid by powder X-ray diffraction (PXRD) analysis. For 200 °C solubility test, a specially designed solubility test apparatus was used. Briefly, the oxide support was mixed with 50 mL of 1 M H₂SO₄ in a zirconium autoclave fitted with a thermocouple. The tightly capped autoclave was pressurized with N₂ gas up to 200 psi and was immersed in a pre-heated silicon oil bath at 200 °C. Inside temperature was monitored using a thermocouple attached to a temperature read-out. Refluxing was continued for 2 h at 200 °C followed by recovery of solution for elemental analysis.

2.3.7. Electrochemical measurement

All electrochemical measurements were performed using a Solartron multistat instrument 1480A, controlled with Corrware software (Scribner Associates Inc., USA). A conventional electrochemical cell at 30 °C was used for measuring both cyclic voltammograms and ORR current–voltage curves. This cell contained three-electrodes: the working, Pt counter, and RHE reference electrodes, respectively.

For the working electrode preparation a uniform layer of catalyst ink was deposited on the gold disk electrode (Au, 0.5 cm diameter, 0.20 cm² geometric surface area, Pine Instruments) and covered with a thin-layer of Nafion[®] ionomer to serve as the catalyst layer. The procedure was as follows: a known amount of catalyst was dispersed in a mixture of isopropyl alcohol (IPA) and de-ionized water (95:5 ratio by volume) followed by sonication in a sonicator bath for 1 h to form a homogeneous catalyst suspension. A required volume of this suspension was then placed on the Au electrode and dried in order to fabricate a thin catalyst layer with a platinum loading of 47.8 $\mu\text{gPt cm}_{\text{geo}}^{-2}$. A Nafion[®] film was cast by pipetting out 7.0 μL of a 100:1 dilution of 5 wt% Nafion[®] ionomer in methanol, on to the catalyst layer coated electrode. The commercial baseline catalyst was 48 wt% Pt/C (TEC10E50E) from TTK.

For electrochemical measurement, this freshly prepared electrode was subjected to a potential cycling in N₂ purged 0.1M HClO₄ electrolyte in the range of 0.05–1.2 V vs. RHE at a scan rate of 20 mV s⁻¹ for 20 cycles. Electrochemical durability testing of the catalysts was carried out following a potential step square-wave method. Briefly, for one cycle, the potential was held at 0.6 V for 30 s and then at 1.2 V for another 30 s, then back to 0.6 V to finish. In this case, each cycle took 60 s. To complete one durability test, 1000 such square wave cycles were needed in N₂-saturated 0.1 M HClO₄ solution. For ORR measurement, the experiment was carried out in O₂-saturated 0.1 M HClO₄ electrolyte at a scan rate of 5 mV s⁻¹ and

at a 1600-rpm electrode rotation speed in the potential range of 0.4–1.2 V vs. RHE. The current–voltage curve at anodic scan was used for ORR activity calculations. The ORR mass activity ($\text{mA mg}_{\text{Pt}}^{-1}$) was calculated using the current at 0.9 V vs. RHE and the Pt loading on the working electrode.

3. Results and discussion

3.1. Structural and morphological characterizations

Fig. 1(a) compares the XRD patterns 25 wt% ($\text{Nb}_{0.07}\text{Ti}_{0.93}\text{O}_2$)-75 wt% C composite support samples synthesized by USP method at different temperatures and reduced at 850 °C for 3 h in H_2 . The XRD data reveal the formation of TiO_2 predominantly in the anatase phase with a high degree of crystallinity, along with the residual rutile phase in some cases, irrespective of the synthesis temperature. The XRD data also shows the absence of extra reflections, i.e. the reflections from Nb_2O_5 or NbO_2 , suggesting proper doping of Nb into TiO_2 lattice. The average crystallite sizes of 25 wt% ($\text{Nb}_{0.07}\text{Ti}_{0.93}\text{O}_2$)-75 wt% C sample were determined by applying the Debye–Scherer equation (Eq. (1)) [15] to full width at half maximum (FWHM) of peak 101 (anatase) at 25.3° and 111(Pt) at 39.76° , respectively.

$$Z = C \frac{\lambda}{B} \cos \theta \tag{1}$$

where Z is the diameter of the average crystallite size in Å, λ is the X-ray wavelength (1.541838 \AA) of Cu $K\alpha$ radiation, θ is the Bragg angle, C is a factor that typically range from 0.9 to 1.0 depending on the crystallite shape, and B is the full width at half maximum (FWHM). The calculated results according Eq. (1) are listed in Table 1. It indicates that the crystallite size of the supports is more or less independent on the synthesis temperature range employed in this work. Generally, the crystallite size increases with increasing synthesis temperature. However, all crystallite sizes of hybrid supports, prepared using the USP method, are quite similar. We assume that TKK-E carbon and metal oxide aerosol are blended so well that the carbon can act as a protective layer against the sintering of metal oxide nanoparticles at higher temperatures.

Fig. 1(b) shows the XRD patterns of 20 wt% $\text{Pt}_{0.62}\text{Pd}_{0.38}$ /25 wt% ($\text{Nb}_{0.07}\text{Ti}_{0.93}\text{O}_2$)-75 wt% C catalyst samples, prepared by the microwave assisted polyol method on 25 wt% ($\text{Nb}_{0.07}\text{Ti}_{0.93}\text{O}_2$)-75 wt% C. The XRD reflections observed for Pt–Pd alloy catalysts are broad due to the smaller crystallite size. The average alloy crystallite size, again calculated using Scherer formula, is slightly varied depending on the type of supports used for catalyst deposition (Table 1). However, given the accuracy of calculation using the

Table 1
Physical properties of 25 wt% ($\text{Nb}_{0.07}\text{Ti}_{0.93}\text{O}_2$)-75 wt% C supports and 20 wt% $\text{Pt}_{0.62}\text{Pd}_{0.38}$ /25 wt% ($\text{Nb}_{0.07}\text{Ti}_{0.93}\text{O}_2$)-75 wt% C catalysts collected at various synthesis temperatures.

Synthesis temperature, (°C)	Conductivity at 25 °C (S cm^{-1})	BET SA ($\text{m}^2 \text{ g}^{-1}$)	Metal oxide crystallite size (nm)	Pt–Pd particle size (nm)
600	2.4	508 ± 6	23.4	3.5
700	2.3	400 ± 11	24.5	5.2
800	2.0	372 ± 4	22.9	3.9

FWHM, there is no significant difference in crystallite sizes of the catalysts prepared using 25 wt% ($\text{Nb}_{0.07}\text{Ti}_{0.93}\text{O}_2$)-75 wt% C supports, which were synthesized at different temperatures.

Representative TEM micrographs of 25 wt% ($\text{Nb}_{0.07}\text{Ti}_{0.93}\text{O}_2$)-75 wt% C support, 20wt% $\text{Pt}_{0.62}\text{Pd}_{0.38}$ /25 wt% ($\text{Nb}_{0.07}\text{Ti}_{0.93}\text{O}_2$)-75 wt% C, and 20 wt% $\text{Pt}_{0.62}\text{Pd}_{0.38}$ /C catalysts are shown in Fig. 2(a–d) along with the high resolution images as insets. The composite support prepared at 600 °C and post treated at 850 °C in H_2 shows the spherical particle morphology at low magnification. As shown in Fig. 2(a), the composite particle size has a broad size distribution and ranges from 250 nm to 2 microns, even though most of the particles were approximately 500 nm in diameter. High magnification images show an irregular morphology (Fig. 2(a) inset) and uniform blend of metal oxide nanocrystals and TKK-E carbon mixture (Fig. 2(b)). Furthermore, from the high resolution images it can be seen that those larger particles consist of aggregations of amorphous carbon particles. Metal oxide nanocrystals exhibit several different morphologies such as spheres, rectangles, and other irregular shapes as well as a wide range of particle sizes (20–60 nm) irrespective of the synthesis temperature. This scenario was similar with no significant difference to those observed in composite supports prepared at 700 and 800 °C.

Fig. 2(c) shows both low and high resolution images of 20wt% $\text{Pt}_{0.62}\text{Pd}_{0.38}$ /25 wt% ($\text{Nb}_{0.07}\text{Ti}_{0.93}\text{O}_2$)-75 wt% C catalyst. It can be clearly seen that $\text{Pt}_{0.62}\text{Pd}_{0.38}$ catalyst particles are uniformly distributed on the support and possess a narrow size distribution. The average $\text{Pt}_{0.62}\text{Pd}_{0.38}$ catalyst particle size, calculated from the data from the high resolution images, was $6.0 \pm 1.5 \text{ nm}$. The similar catalyst distribution but slightly lower particle size (avg. 4.5 nm) can be observed for 20 wt% $\text{Pt}_{0.62}\text{Pd}_{0.38}$ /C (Fig. 2(d)).

3.2. Evaluation of actual carbon content of hybrid supports by TGA analysis

TGA analysis was employed to verify the actual carbon content in the USP prepared hybrid supports. Fig. 3 represents the plots of

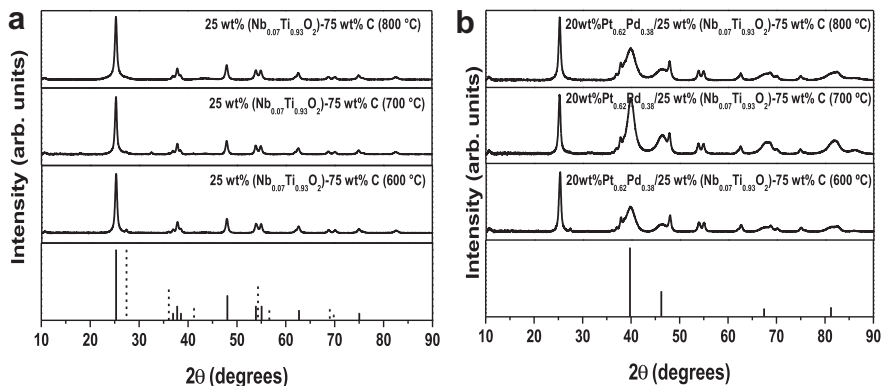


Fig. 1. XRD patterns of the (a) 25 wt% ($\text{Nb}_{0.07}\text{Ti}_{0.93}\text{O}_2$)-75 wt% C supports synthesized by USP method at temperatures from 600 to 800 °C followed by reduction at 850 °C for 3 h in H_2 , and (b) 20wt% $\text{Pt}_{0.62}\text{Pd}_{0.38}$ /25 wt% ($\text{Nb}_{0.07}\text{Ti}_{0.93}\text{O}_2$)-75 wt% C catalysts prepared by microwave assisted polyol synthesis. The bottom vertical lines indicate the peak positions of anatase [solid (a)], rutile [dashed (a)], and Pt [solid (b)].

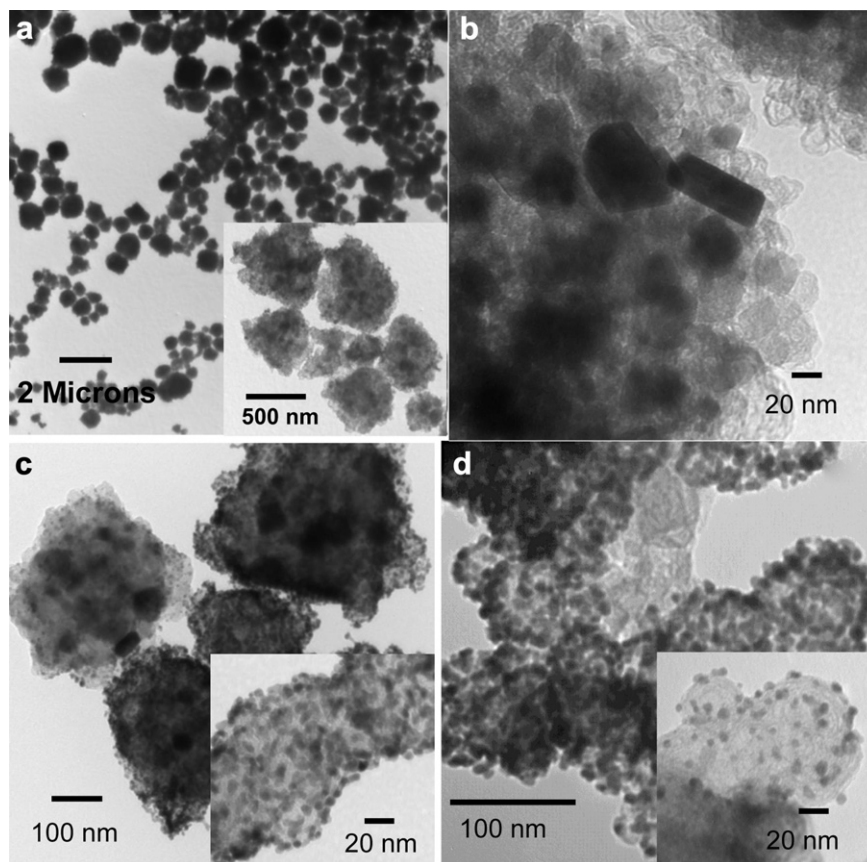


Fig. 2. Transmission electron micrographs of (a) 25 wt% ($\text{Nb}_{0.07}\text{Ti}_{0.93}\text{O}_2$)-75 wt% C support synthesized at 600 °C (low mag.), (b) high magnification image of 25 wt% ($\text{Nb}_{0.07}\text{Ti}_{0.93}\text{O}_2$)-75 wt% C support that shows metal oxide particles embedded in carbon matrix, (c) 20 wt% $\text{Pt}_{0.62}\text{Pd}_{0.38}$ /25 wt% ($\text{Nb}_{0.07}\text{Ti}_{0.93}\text{O}_2$)-75 wt% C, and (d) 20 wt% $\text{Pt}_{0.62}\text{Pd}_{0.38}$ /C. Insets to each image shows high magnification micrographs of corresponding TEM image.

thermogravimetric analysis (TGA) of 25 wt% ($\text{Nb}_{0.07}\text{Ti}_{0.93}\text{O}_2$)-75 wt% C support synthesized at different temperatures (600–800 °C), recorded by heating the samples in air of a temperature range of 50–700 °C. It can be seen that the loss of weight initiates at about 450 °C for all samples and reached a completion upon holding isothermally at 550 °C for 30 min. Further heating shows no weight

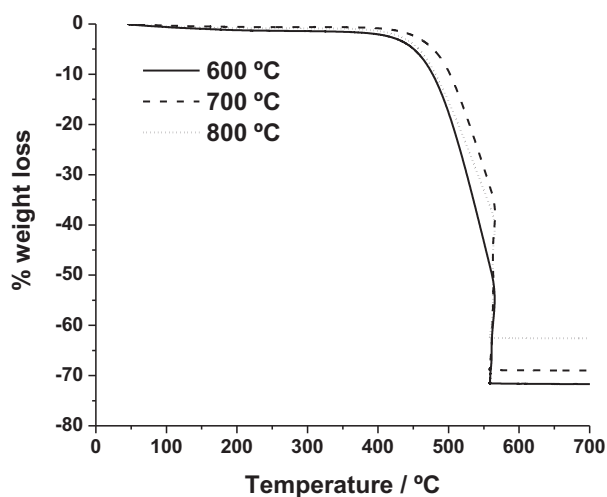


Fig. 3. Thermogravimetric analysis data plots acquired for 25 wt% ($\text{Nb}_{0.07}\text{Ti}_{0.93}\text{O}_2$)-75 wt% C composite supports prepared at different synthesis temperatures. The percentage weight loss represents the percentage of carbon present in the hybrid support.

loss, indicating that all the carbon has been oxidized. Due to the high thermal stability of metal oxide phase, weight loss should be mainly associated to carbon content available in the hybrid support. The weight loss derived from TGA data ranges from 63 to 72 wt% while the support prepared at 600 °C shows the highest loss among all the samples tested. The actual carbon content present in the USP-prepared supports was in the order of samples prepared at 600 > 700 > 800 °C. It is due to the possible carbon oxidation by remaining oxygen at high temperatures. This may be one of the possible reasons why there is a lower carbon content in support prepared at 800 °C than that of samples prepared at 600 °C. The experimentally determined carbon content is closely resembled the nominal (75%). Therefore, we can conclude that the synthesis conditions applied during the USP synthesis allow us to incorporate known amount of carbon into hybrid support materials with approximately 95% accuracy.

3.3. Surface area analysis

Fig. 4(a–b) represents the nitrogen adsorption-desorption isotherms, and the percentage pore size distribution plots for 25 wt% ($\text{Nb}_{0.07}\text{Ti}_{0.93}\text{O}_2$)-75 wt% C composite supports, synthesized at temperatures range from 600 to 800 °C. The surface areas calculated by the Brunauer–Emmet–Teller (BET) method were relatively higher and range from 372 to 508 $\text{m}^2 \text{g}^{-1}$, as listed in Table 1. The 25 wt% ($\text{Nb}_{0.07}\text{Ti}_{0.93}\text{O}_2$)-75 wt% C support synthesized at 600 °C shows the highest BET area (508 $\text{m}^2 \text{g}^{-1}$). A major fraction of the surface area is contributed by carbon. The presence of lower carbon content may account for the lower surface area in the composites

prepared at higher temperatures. In addition, effective filling of pore sites of carbon by metal oxides and decrease in pore volume and pore size distribution at higher temperatures may be responsible for lower surface area observed in samples prepared at higher temperatures. As shown in Fig. 4(b), the supports show a broad pore size distribution, calculated by Barrett–Joyner–Halenda method, that ranges from 5 to 100 nm in diameter. However, the majority of the pores appear to be in the meso-regime (2–50 nm), therefore they are quite easily accessible to catalyst nanoparticles.

3.4. Chemical stability tests of 25 wt% (Nb_{0.07}Ti_{0.93}O₂)-75 wt% C composite supports

Chemical stability in terms of solubility and phase integrity of 25 wt% (Nb_{0.07}Ti_{0.93}O₂)-75 wt% C composite support was evaluated in 1 M H₂SO₄ at two different temperatures 95 and 200 °C, and percentage solubility have been summarize in Table 2. The total percentage solubility of Nb and Ti in the composite was significantly low at both 95 (0.5%) and 200 °C (0.85%) under the applied experimental conditions. This low solubility of Nb-doped TiO₂ in acidic solution suggests that it is a favorable component that can be included in composite supports as well as used in fuel cell applications.

3.5. Electrochemical characterization

For electrochemical characterization, Fig. 5(a) shows the cyclic voltammograms (CVs) of Pt_{0.62}Pd_{0.38} catalyst deposited on three 25 wt% (Nb_{0.07}Ti_{0.93}O₂)-75 wt% C supports synthesized at 600, 700, and 800 °C, respectively. The CVs show a hydrogen adsorption–desorption and oxidation–reduction regions. It is noteworthy that the hydrogen adsorption–desorption region is smooth and shows no sharp peaks. Normally, Pd catalysts show sharp peaks in hydrogen absorption–desorption region due to hydrogen gas storage ability inside the Pd lattice, and the inserted hydrogen inside Pd sites can get oxidized at a low potentials (~0 V) [16]. The absence of corresponding sharp peaks in absorption–desorption region is indicative of proper alloying of Pd with Pt. The electrical double layer of 20wt%Pt_{0.62}Pd_{0.38}/25 wt% (Nb_{0.07}Ti_{0.93}O₂)-75 wt% C synthesized at 600 °C, is the broadest and becomes smaller with increasing temperature. The high surface area and porosity (503 m² g^{−1}) of 20wt%Pt_{0.62}Pd_{0.38}/25 wt% (Nb_{0.07}Ti_{0.93}O₂)-75 wt% C synthesized at 600 °C should be responsible for the broader double layer [17]. Similarly, commercial 48 wt% Pt/C (TKK), where TKK's E type carbon is the support and 20 wt% Pt_{0.62}Pd_{0.38}/C (also using TKK-E carbon) shows

Table 2

Solubility data determined by ICP/MS analysis of 25 wt% (Nb_{0.07}Ti_{0.93}O₂)-75 wt% C support refluxed at 95 and 200 °C in 1 M H₂SO₄ for 24 and 2 h, respectively.

Metal	Percentage solubility (wt%)	
	95 °C	200 °C
Ti	0.37	0.4
Nb	0.13	0.45

the thinnest double layer out of all the catalysts (Fig. 6(a)). As evidenced from CVs of Fig. 6(a), oxide reduction potential of 20wt%Pt_{0.62}Pd_{0.38}/25 wt% (Nb_{0.07}Ti_{0.93}O₂)-75 wt% C synthesized at 600 °C is 0.784 V and 40 mV more positive than the oxide reduction potential of commercial Pt/C. This may be indicative that the 20wt%Pt_{0.62}Pd_{0.38}/25 wt% (Nb_{0.07}Ti_{0.93}O₂)-75 wt% C is less oxophilic than Pt/C [18]. Although the experimental data supports complete alloying between Pt and Pd, the effect of Pd on hydrogen adsorption and desorption onto PtPd alloy catalyst sites could introduce significant unknowns into ESA calculations. Thus determination of PtPd electrochemical surface area (ESA) using the same constants as for Pt ESA calculations does not make much sense. Therefore, we did not go further in determining PtPd ESA in this paper. It follows that specific activity using ESA values is also not reported here.

The ORR electrocatalytic activities and stabilities of the catalysts were tested using a rotating disk electrode technique in an O₂-saturated 0.1 M HClO₄ solution at 30 °C. The current–voltage curves, recorded at 1600 rpm electrode rotation rate using 20wt%Pt_{0.62}Pd_{0.38}/25 wt% (Nb_{0.07}Ti_{0.93}O₂)-75 wt% C synthesized at 600–800 °C, 20wt%Pt/25 wt% (Nb_{0.07}Ti_{0.93}O₂)-75 wt% C, Pt_{0.62}Pd_{0.38}/C (TKK-E), as well as commercial Pt/C are shown in Figs. 5(b) and 6(b), respectively and a summary table of catalyst names and abbreviations used are given in Table 3. The ORR mass activities were calculated using the currents measured at 0.9 V vs. RHE of the anodic sweep at 1600 rpm. It can be seen that the onset potentials are located in the range of 1.04–1.05 V for all the composite supported catalysts, but the onset potential for commercial Pt/C (TKK) and Pt_{0.62}Pd_{0.38}/C (TKK-E) is slightly lower. All ORR data are listed in Table 4. It can be seen that the composite supported Pt_{0.62}Pd_{0.38} alloy catalysts show a similar ORR mass activity in the narrow range of 155–157 mA mg_{Pt}^{−1}. However, compared to both the commercial Pt/C and Pt_{0.62}Pd_{0.38}/C (TKK-E), these composite supported catalysts are 32% and 17% more active, respectively. The activity of 20wt%Pt/25 wt% (Nb_{0.07}Ti_{0.93}O₂)-75 wt% C catalyst is lower than that of 20wt%Pt_{0.62}Pd_{0.38}/25 wt% (Nb_{0.07}Ti_{0.93}O₂)-75 wt% C alloy catalyst but slightly higher than commercial Pt/C (129 vs. 110 mA mg_{Pt}^{−1}). This observation may suggest that the metal oxide/carbon composite

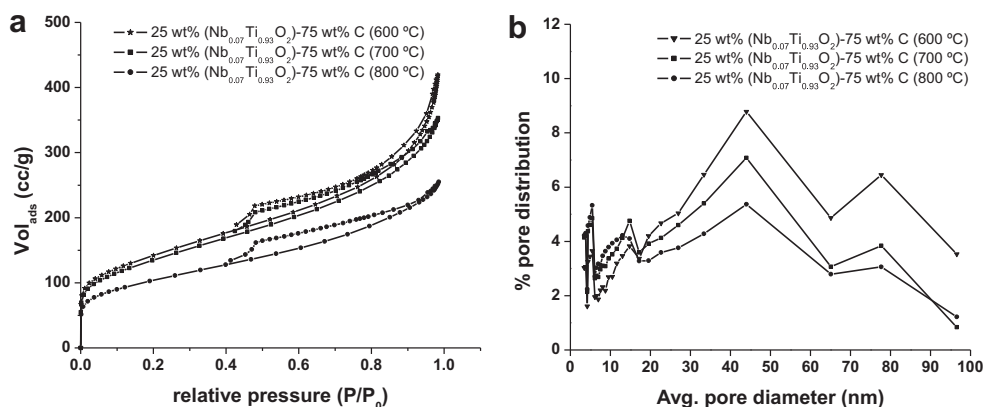


Fig. 4. Nitrogen adsorption–desorption isotherms (a) and pore size distribution plots as a function of average pore diameter (b) of 25 wt% (Nb_{0.07}Ti_{0.93}O₂)-75 wt% C support synthesized in the temperatures range from 600 to 800 °C.

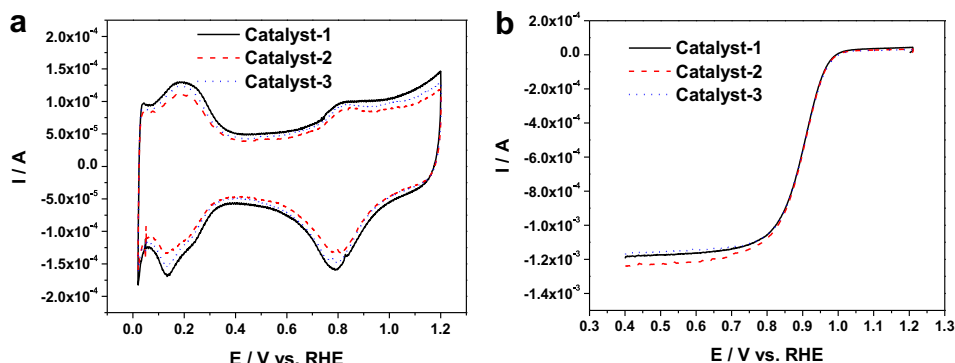


Fig. 5. (a) Cyclic voltammograms and (b) ORR linear sweep voltammograms recorded for 20 wt%Pt_{0.62}Pd_{0.38}/25 wt% (Nb_{0.07}Ti_{0.93}O₂)-75 wt% C catalysts synthesized at three different temperatures in N₂-saturated 0.1 M HClO₄ and in O₂-saturated 0.1 M HClO₄, respectively at 30 °C.

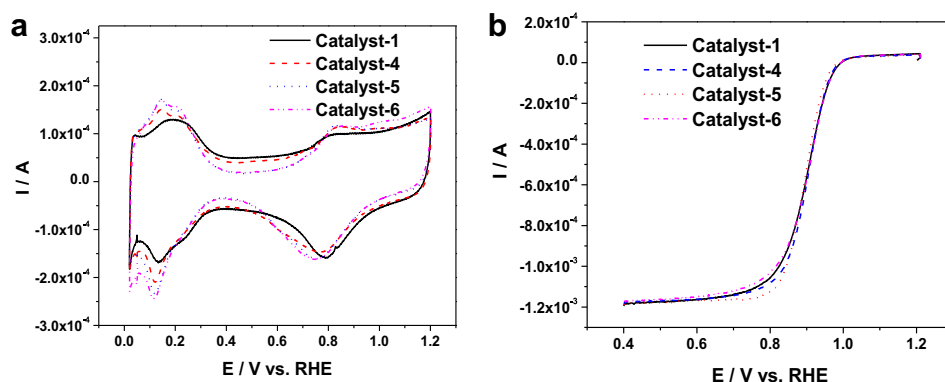


Fig. 6. (a) Cyclic voltammograms and (b) ORR linear sweep voltammograms recorded for different catalysts in N₂-saturated 0.1 M HClO₄ and in O₂-saturated 0.1 M HClO₄, respectively at 30 °C.

support could have a synergistic effect toward ORR activity. However, even though the catalytic activity of 20wt%Pt_{0.62}Pd_{0.38}/25 wt% (Nb_{0.07}Ti_{0.93}O₂)-75 wt% C catalysts is higher than that of commercial Pt/C, its stability is less than Pt/C or 20wt%Pt_{0.62}Pd_{0.38}/C. The low stability observed in this work is different from that has been reported for Nb–TiO₂ supported Pt catalyst in our group's previous publication and other groups' reports, where some better stabilities were observed when compared to commercial Pt/C catalyst. However, it should be noted that the mass activity reported in those papers is very low and close to 20 mA mgPt⁻¹ [6]. It seems that the factors affecting catalyst's stability are quite complicated and, in this case, need to be explored. However, we believe that the support and catalyst preparation can strongly affect the performances. In order to enhance the conductivity of composite supports, they were heat treated in a reducing atmosphere prior to catalysts deposition. The heat treatment creates a fraction of Ti³⁺ on/near the TiO₂ surface, which accounts for higher conductivity. During electrochemical testing, it is possible that these Ti³⁺ to undergo

electrochemical oxidation into Ti⁴⁺ creating a nonconductive layer of TiO₂, that may prevent the communication between catalyst and support leading to a drop in activity. However, a detailed exploration has to be carried out to properly understand the factors that cause catalyst degradation.

For ORR kinetic measurement, Fig. 7(a) shows current–voltage curves recorded at different electrode rotation rates using 20wt% Pt_{0.62}Pd_{0.38}/25 wt% (Nb_{0.07}Ti_{0.93}O₂)-75 wt% C catalyst synthesized at 600 °C in O₂-saturated 0.1 M HClO₄ electrolyte at the potential scan rate of 5 mV s⁻¹. The three regions can be clearly observed such as a diffusion-limited region from 0.4 to 0.7 V (RHE), a mixed diffusion-kinetic limitation region from 0.7 to 0.85 V followed by a purely kinetic controlled region above 0.85 V. The ORR current

Table 3

Summary of catalyst names, support processing temperature, and abbreviations used in the legends of electrochemical data plots.

Catalyst name	Support processing temperature/°C	Abbreviation used
20wt%Pt _{0.62} Pd _{0.38} /25 wt% (Nb _{0.07} Ti _{0.93} O ₂)-75 wt% C	600	Catalyst 1
	700	Catalyst 2
	800	Catalyst 3
20wt%Pt/25 wt% (Nb _{0.07} Ti _{0.93} O ₂)-75 wt% C	600	Catalyst 4
20wt%Pt _{0.62} Pd _{0.38} /TKK-E	Commercial	Catalyst 5
48wt%Pt/C(TKK)	Commercial	Catalyst 6

Table 4

Summary of ORR mass activities of various catalyst prepared using USP synthesized supports. Activity of commercial Pt/C catalyst is also given for comparison.

Catalyst	ORR mass activity @ 0.9 V (mA mgPt ⁻¹)	
	Initial	% Loss after durability
48 wt%Pt/C (TKK)	110	33.0
20 wt%Pt/25 wt% (Nb _{0.07} Ti _{0.93} O ₂)-75 wt% C (600 °C)	129	39.0
20 wt%Pt _{0.62} Pd _{0.38} /TKK-E	132	40.0
20 wt%Pt _{0.62} Pd _{0.38} /25 wt% (Nb _{0.07} Ti _{0.93} O ₂)-75 wt% C (600 °C)	157	51.0
20 wt%Pt _{0.62} Pd _{0.38} /25 wt% (Nb _{0.07} Ti _{0.93} O ₂)-75 wt% C (700 °C)	155	52.0
20 wt%Pt _{0.62} Pd _{0.38} /25 wt% (Nb _{0.07} Ti _{0.93} O ₂)-75 wt% C (800 °C)	157	49.0

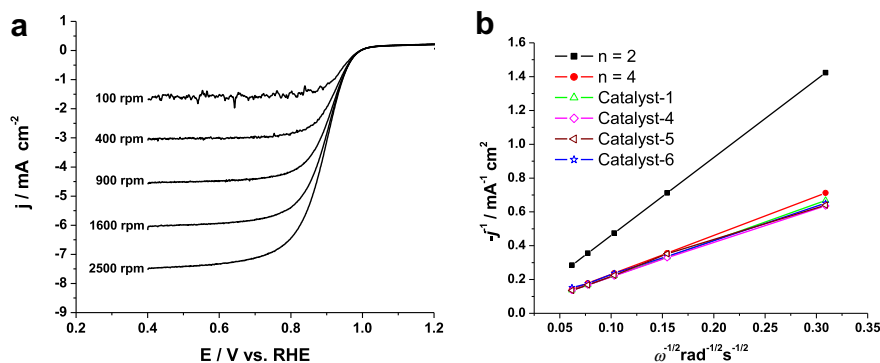


Fig. 7. (a) ORR linear sweep voltammograms recorded at 5 mV s^{-1} and various rotation rates on the 20 wt%Pt_{0.62}Pd_{0.38}/25 wt% (Nb_{0.07}Ti_{0.93}O₂)-C75wt% catalyst synthesized at 600 °C, and (b) Koutecky–Levich plots at different potentials for ORR in the anodic sweep of various catalysts, in O₂-saturated 0.1 M HClO₄ solution at 30 °C.

density j can be expressed by the Koutecky–Levich equation [8,17,19]:

$$j = \left(\frac{1}{j_k} + \frac{1}{j_d} + \frac{1}{j_f} \right)^{-1} \quad (2)$$

where j_d is the diffusion limiting current density, which can be expressed as:

$$j_d = 0.62nFD_{\text{O}_2}^{\frac{2}{3}}C_{\text{O}_2}\nu^{-\frac{1}{6}}\omega^{\frac{1}{2}} \quad (3)$$

In Eq. (2), j_k is the kinetic current density; j_f is the diffusion-limiting current density through the Nafion[®] layer. In Eq. (3), n is the overall number of transferred electrons in the ORR process, F is the Faraday constant ($96,485 \text{ C mol}^{-1}$), D_{O_2} is the diffusion coefficient of molecular oxygen in the solution, C_{O_2} is the concentration of molecular oxygen in 0.1 M HClO₄, ν is the kinematic viscosity ($9.87 \times 10^{-3} \text{ cm}^2 \text{ s}^{-1}$), and ω is the angular frequency of rotation derived from $\omega = 2\pi f/60$, f is the rotation rate in rpm. Assuming that the thickness of Nafion[®] layer is too thin to impose sufficient resistance [20], Eq. (2) can be simplified into Eq. (4):

$$j = \left(\frac{1}{j_k} + \frac{1}{j_d} \right)^{-1} \quad (4)$$

A Koutecky–Levich plot, which is the plot of j^{-1} vs. $\omega^{-1/2}$, at a fixed potential should be a linear relationship in which slope and intercept represent a constant and j_k^{-1} , respectively. Fig. 7(b) shows the Koutecky–Levich plots at different potentials for ORR in the anodic sweep on 20 wt%Pt_{0.62}Pd_{0.38}/25 wt% (Nb_{0.07}Ti_{0.93}O₂)-75 wt% C catalyst synthesized at 600 °C, 20 wt%Pt/25 wt% (Nb_{0.07}Ti_{0.93}O₂)-75 wt% C catalyst synthesized at 600 °C, 20wt%Pt_{0.62}Pd_{0.38}/C (TKK-E), and commercial 48-wt% Pt/C (TKK), and Pt₆₂Pd₃₈/TKK-E catalysts. Theoretical Koutecky–Levich plots for two- and four-electron processes are also plotted for comparison. It can be seen that all the lines are linear and the derived plots for tested catalysts are closely in line with the theoretical plot for a four-electron process. This indicates that the oxygen reduction reaction proceeds through a four-electron transfer process for Pt₆₂Pd₃₈ catalysts analyzed in this study. Therefore, we surmise that the Pt_{0.62}Pd_{0.38} catalysts are active for ORR forming H₂O without generating side product peroxide.

4. Conclusion

The Ultrasonic Spray Pyrolysis (USP) method was successfully employed to synthesize Nb-doped TiO₂/carbon composite supports 25 wt% (Nb_{0.07}Ti_{0.93}O₂)-75 wt% C at different temperatures. These

composite materials were used as the supports for Pt_{0.62}Pd_{0.38} alloy catalysts, which were synthesized using a microwave-assisted polyol reduction method. The synthesized catalysts were physically characterized using several physical methods such as XRD, TEM, BET surface area analysis, TGA, as well as ICP-MS in terms of material morphologies, chemical/thermal stabilities as well as the electronic conductivities. It was found that these composite materials are stable in a PEM fuel cells environment of mild acid (1 M H₂SO₄) and a temperature range of 95–200 °C.

The composite catalysts, 20 wt%Pt_{0.62}Pd_{0.38}/25 wt% (Nb_{0.07}Ti_{0.93}O₂)-75 wt% C, synthesized at different temperatures were electrochemically tested for both ORR mass activity and stability in acidic solution and the obtained results were compared to those of commercial 48-wt% Pt/C (TKK) and home-made 20 wt% Pt_{0.62}Pd_{0.38}/C (TKK-E) catalyst. The composite catalysts showed 35% higher mass activity towards ORR. This result may suggest that this composite supported catalyst may be feasible for using in PEM fuel cell cathode oxygen reduction reaction.

Acknowledgement

This work is part of Canadian National Technological Development Program (TDP), financially funded by National Research Council of Canada (NRC), AFCC Automotive Fuel Cell Cooperation Corp, Ballard Power Systems, and led by Mr. Allan Guest of NRC. The authors would like to express their gratitude to Dr. Dave Ghosh, Dr. Rod McMillan, Dr. Barry MacDougall, Dr. Christina Bock, and Dr. Chaojie Song from NRC, Mrs. Shanna Knights from Ballard, and Dr. Harmeet Chhina from AFCC Automotive Fuel Cell Cooperation Corp.

References

- [1] W. Lubitz, W. Tumas, Chem. Rev. 107 (2007) 3900–3903.
- [2] S.-Y. Huang, P. Ganesan, B.N. Popov, Appl. Catal. B 96 (2010) 224–231.
- [3] S.G. Chalk, J.E. Miller, J. Power Sources 159 (2006) 73–80.
- [4] K.-W. Park, K.-S. Seol, Electrochem. Commun. 9 (2007) 2256–2260.
- [5] L. Chevallier, A. Bauer, S. Cavaliere, R. Hui, J. Rozière, D.J. Jones, Appl. Mater. Interf. 4 (2012) 1752–1759.
- [6] A. Bauer, R. Hui, A. Ignaszak, J. Zhang, D.J. Jones, J. Power Sources 210 (2012) 15–20.
- [7] Y.-J. Wang, D. Wilkinson, J. Zhang, Dalton Trans. 41 (2012) 1187–1194.
- [8] Z. Li, L. Zhang, H. Liu, M. Pan, L. Zan, J. Zhang, Electrochim. Acta 55 (2010) 4403–4411.
- [9] M. Garden, M. Lukaszewski, G. Jerkiewicz, A. Czerwinski, Electrochim. Acta 53 (2008) 7583–7593.
- [10] F. Alcaide, G. Álvarez, P.L. Cabot, O. Miguel, A. Querejeta, Int. J. Hydrogen Energy 35 (2010) 11634–11641.
- [11] G.L. Messing, S.-C. Zhang, G.V. Jayanthi, J. Am. Ceram. Soc. 76 (1993) 2707–2726.
- [12] W.-H. Suh, A.R. Jang, Y.-H. Suh, K.S. Suslick, Adv. Mater. 18 (2006) 1832–1837.
- [13] V. Jokanović, A.M. Spasić, D. Uskoković, J. Colloid Interf. Sci. 278 (2004) 342–352.
- [14] W.-H. Suh, K.S. Suslick, J. Am. Chem. Soc. 127 (2005) 12007–12010.

- [15] K. Senevirathne, A. Burns, M.E. Bussell, S. Brock, *Adv. Funct. Mater.* 17 (2007) 3933–3939.
- [16] M. Wu, P.K. Shen, Z. Wei, S. Song, M. Nie, J. *Power Sources* 166 (2007) 310–316.
- [17] Q. He, S. Mukerjee, *Electrochim. Acta* 55 (2010) 1709–1719.
- [18] W.J. Khudhayer, N.N. Kariuki, X. Wang, D.J. Myers, A.U. Shaikh, T. Karabacak, *J. Electrochem. Soc.* 158 (2011) B1029–B1041.
- [19] E. Higuchi, H. Uchida, M. Watanabe, *J. Electroanal. Chem.* 583 (2005) 69–76.
- [20] U.A. Paulus, A. Wokaun, G.G. Scherer, T.J. Schmidt, V. Stamenkovic, N.M. Markovic, P.N. Ross, *Electrochim. Acta* 47 (2002) 3787–3798.